PERGAMON

International Journal of Heat and Mass Transfer 42 (1999) 1217–1235

International Journal of HEAT and MASS TRANSFER

Effect of an oblique plate on the heat transfer enhancement of mixed convection over heated blocks in a horizontal channel

Horng-Wen Wu*, Shiang-Wuu Perng

Department of Naval Architecture and Marine Engineering, National Cheng Kung University, Tainan, Taiwan, Republic of China

Received 22 January 1998; in final form 20 July 1998

Abstract

This study presents a numerical investigation on heat transfer enhancement of mixed convective flow in a horizontal block-heated channel. The heat transfer enhancement in this study has been accomplished by the installation of an oblique plate for internal flow modification induced by vortex shedding. The oblique angle of the plate is changed (30–90°) under Reynolds numbers (260–530) and Grashof numbers (0–3 200 000) for the purpose of investigating the heat transfer performance. The results show that the installation of an oblique plate in cross-flow above an upstream block can effectively enhance the heat transfer performance of mixed convection in the horizontal channel flow.

Nomenclature

A diffusion matrix of energy equation
C_p pressure coefficient ($2\int Pds/\int ds$)
D divergence matrix
d length of the oblique plate
ds surface area increment along the oblique plate
f_s frequency of the vortex shedding
Gr Grashof number ($g\beta qw^4/kv^2$)
H pressure gradient matrix
H channel wall-to-wall spacing
h height of the block
K conduction matrix
k thermal conductivity
L channel length
M mass matrix
Nu Nusselt number
$\bar{N}u$ time-mean Nusselt number ($\int Nu\, dt/\int dt$)
n normal vector
n_g unit vector along the gravity direction
P pressure vector of nodal points
P dimensionless pressure (p^*/pu_∞^2)
p^* pressure
Pr Prandtl number (v/λ)
Q imposition vector of heat-flux boundary conditions
q heat flux at the block boundary
Re Reynolds number ($u_\infty w/v$)
S diffusion matrix of the momentum equation
St Strouhal number ($d(\sin\omega)f_s/u_\infty$)
T^* temperature
T_∞ uniform inlet temperature
t dimensionless time ($t^*/(w/u_\infty)$)
Δt dimensionless time increment
t^* time
u velocity vector
U velocity vector of nodal points
$\tilde{U}$, $\hat{U}$ intermediate velocity matrix
u_∞ uniform inlet velocity
u, v dimensionless velocity components ($u = u^*/u_\infty$, $v = v^*/v_\infty$)
u^*, v^* velocity components
w width of the block
x, y dimensionless x^*, y^* coordinates ($x = x^*/w$, $y = y^*/w$)
x^*, y^* physical coordinates.

Greek symbols
λ thermal diffusivity
ω inclined angle of a plate
Θ temperature vector of nodal points
θ dimensionless temperature ($(T^* - T_\infty^*)/(qw/k)$)
v kinematic viscosity of fluid

* Corresponding author. Tel.: 00886 06 274 7018; fax: 00886 06 274 7019; e-mail: whw@nmdec.nm.ncku.edu.tw

0017–9310/98/$ - see front matter
PII: S0017–9310(98)00247–6

Superscripts
$n+1$, n, $n-1$ $n+1$th, nth, $n-1$th time step.

1. Introduction

Electronic devices have become more compact and hence densely packaged in response to the demands for cost savings and higher performance. The trends thus reintroduced the thermal problem [1, 2]. Improvements in cooling methods are required in order to avoid unacceptable temperature rises. The air cooling of an array of rectangular sources is of particular interest. Mixed convection has recently received considerable attention because the heat fluxes are increased within electronic components.

Mixed convection in horizontal channels is of interest in cooling of local heat sources encountered in electronic devices. Kennedy and Zebib [3] reported mixed convection between horizontal parallel plates with a local heat source flash-mounted on the horizontal plate. They showed the heat transfer characteristics and flow pattern resulting from four cases of heat source locations. Kang et al. [4] investigated experimentally mixed convective transport from an isolated source located on a horizontal adiabatic plate. The dependence of the heat transfer rate on the mixed convection parameter and on the thickness of the heated element were investigated. However, the effect of thermal wake interaction could not be clarified because single heat source configurations were considered. Bratten and Patankar [5] studied numerically the laminar mixed convection in shrouded arrays of heated rectangular blocks mounted on the horizontal shrouds, spaced periodically in the spanwise direction. Kim et al. [6] presented numerical results on the mixed convection from multiple-layered boards with cross-streamwise periodic boundary conditions in a horizontally-oriented channel and a vertically-oriented channel.

Several papers [7–14] have dealt with the use of vortex generators to enhance heat transfer in the forced convection regime. Sparrow et al., [7] experimentally investigated the effect of implemented barriers in arrays of rectangular modules and reported significant improvement in the heat transfer coefficient of the module in the second row downstream of the barrier. Myrum et al. [8–10] have conducted a series of experiments on dealing vortex generators (circular rods) induced enhancement of heat transfer from ribbed ducts in which different generator configurations were studied by changing rod diameter, rod-rib spacing and rod-rod spacing. Ratts et al. [11] presented an experimental study on internal flow modification induced by vortex shedding from cylinders in air cross flow and its effect on cooling of an array of chips. Chou and Lee [12] conducted an experimental work on the possibility of reducing flow non-uniformities in LSI packages by vortex generating from a rectangular plate on the top of a down-stream chip. Karniadakis et al. [13] used the isoparametric spectral element method to investigate the heat transfer enhancement by placing eddy promoter cylinders in a grooved-channel flow. Nigen and Amon [14] demonstrated the effectiveness of self-sustained oscillatory flows in enhancing convective cooling of surface-mounted packages through a comparison of maximum junction temperatures.

Although many studies have been conducted on enhancement techniques for forced convection, there are few reports on natural convection. One of enhancement techniques is to modify flow pattern through vortex shedding employing little on mixed convection enhancement. The enhancement technique to be investigated here is the employment of an oblique plate to generate vortex shedding in a horizontal block-heated channel. Examining the efficacy of the enhancement technique for mixed convection is a motivation to us from practical consideration. The present research is a numerical study of mixed convection enhancement. The purpose of this paper is to quantify the influence of oblique angle of the plate on heat transfer enhancement by changing Reynolds number and Grashof number. This paper describes a semi-implicit finite element study that investigated flow modification by means of vortex shedding generated by an oblique plate and its effect on heat transfer enhancement of mixed convection occurring in heated blocks. Semi-implicit finite element method with the projection technique proposed by Ramaswany et al. [15, 16] is a powerful numerical method for unsteady incompressible thermal flows. They showed that this method generally requires much less computer storage and computation time than the conventional finite element methods. The results of this study may be of interest to engineers attempting to develop thermal control of electronic devices and to researchers interested in the flow-modification aspects of heat transfer enhancement of mixed convection in a horizontal channel.

2. Numerical modelling

The physical problem considered in this study is the two-dimensional mixed convective flow of an incompressible fluid passing over heated blocks mounted on one side of the horizontal channel as shown in Fig. 1. The geometrical relations for this study are set forth: $H/w = 2.5$, $L/w = 25$, $d/w = 0.45$, and $h/w = 0.5$. In the present treatment, all the physical properties of the fluid are taken to be constant. Utilizing the Boussineq approximation [17], we can express the governing equations in properly dimensionless form as follows

$$\nabla \cdot \mathbf{u} = 0. \tag{1}$$

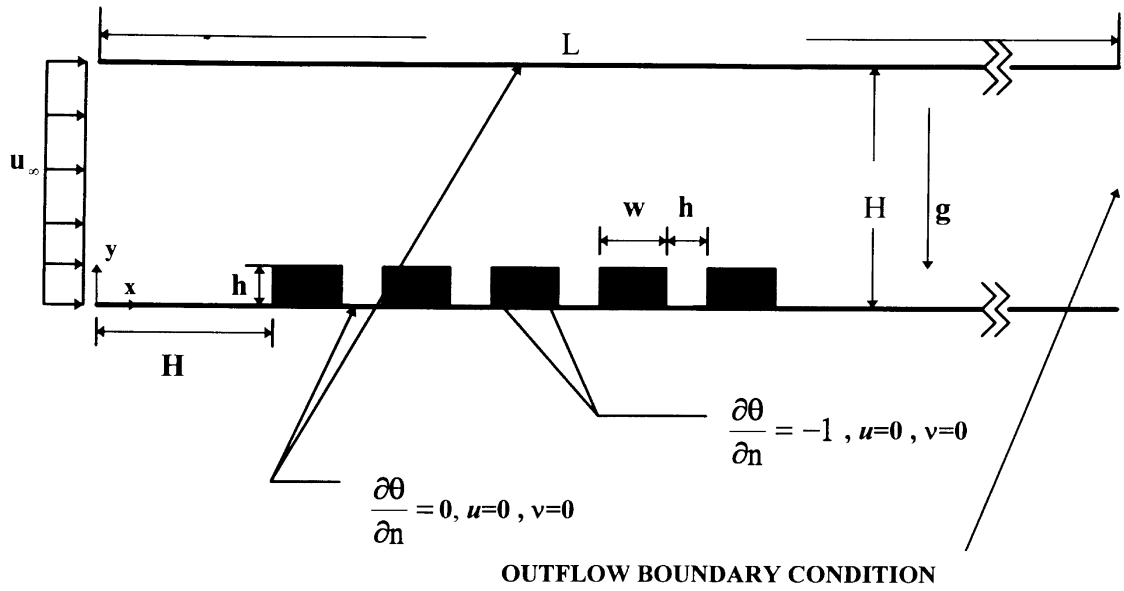

(a)

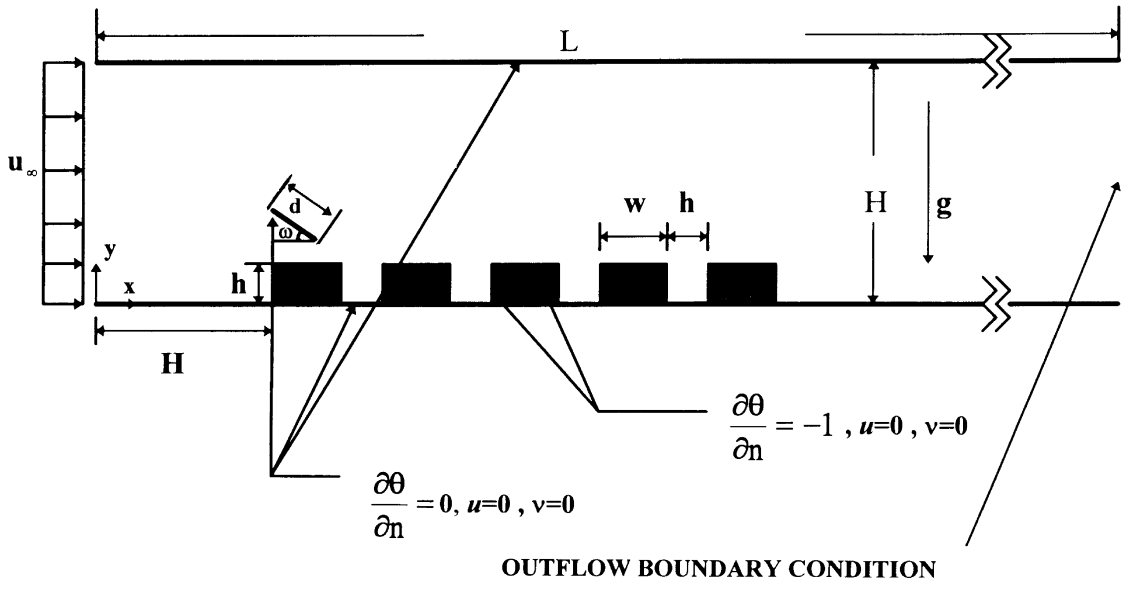

Fig. 1. The geometrics considered here: (a) without an oblique plate, (b) with an oblique plate above the first block.

$$\frac{\partial \mathrm{u}}{\partial t}+(\mathrm{u}\cdot\nabla)\mathrm{u}=-\nabla P+\frac{1}{Re}\nabla^2\mathrm{u}+\frac{Gr\theta}{Re^2}\mathrm{n_g} \tag{2}$$

$$\frac{\partial \theta}{\partial t}+(\mathrm{u}\cdot\nabla)\theta=\frac{1}{RePr}\nabla^2\theta \tag{3}$$

where u is the velocity, P is the pressure, and $\mathrm{n_g}$ represents unit vector along the gravity direction.

The initial conditions are

$$\text{for } t=0, \text{in the region, } u=v=\theta=0. \tag{4}$$

We use the following boundary conditions for computations. Cases with and without the oblique plate have the same external boundary conditions; uniform inflow with $u=1$, $v=0$; no-slip boundary conditions $u=0$ and $v=0$ on the upper and lower channel surfaces; and a standard outflow boundary condition $\partial u/\partial x=0$ and $\partial v/\partial x=0$ across the outflow plane. The temperature field satisfies $\theta=0$ at the inflow boundary, $\partial\theta/\partial n=-1$ along the block (heat-producing) surface, and $\partial\theta/\partial n=0$ along the other surfaces. The oblique plate represents a no-slip surface $u=0$ and $v=0$ with zero temperature gradient $\partial\theta/\partial n=0$.

The conventional Galerkin finite element spatial discretization of eqn (1) to eqn (9) or eqn (10) leads to the following systems of couple ordinary equations [15, 16]

$$\mathrm{M}\frac{\mathrm{dU}}{\mathrm{d}t}+\mathrm{HP}+\frac{1}{Re}\mathrm{S(U)}+\mathrm{K(U)U}=\frac{Gr}{Re^2}\mathrm{M}\Theta\delta_{\mathrm{i2}} \tag{5}$$

$$\mathrm{M}\frac{\mathrm{d}\Theta}{\mathrm{d}t}+\frac{1}{RePr}\mathrm{A}\Theta+\mathrm{K(U)}\Theta=\frac{1}{RePr}\mathrm{Q} \tag{6}$$

and

$$\mathrm{DU}=0 \tag{7}$$

where M, K, H and $\mathrm{D}=\mathrm{H}^T$ are the mass, convection, pressure gradient, and divergence matrices, respectively. S is the diffusion matrix of the momentum equation, and A is the diffusion matrix of the energy eqn. Vectors U, Θ, and P represent finite element solutions for velocity, temperature, and pressure, respectively. The right hand side vector Q results from the imposition of heat-flux boundary conditions.

The following fully discretized Galerkin eqns may be derived by adopting a second-order Adams–Bashforth for the advection term and implicit Euler representation for the diffusion term, but predominantly considering the concepts of the projection approach [15].

2.1. Advection phase

The phase allows us to determine an intermediate velocity field $\hat{\mathrm{U}}^{n+1}$ from U^n starting with U_0 for $n=0$, utilizing the explicit Adams–Bashforth method for the nonlinear convective terms.

$$\mathrm{M}\hat{\mathrm{U}}^{n+1}=\mathrm{MU}^n-\Delta t\left[\frac{3}{2}\mathrm{K(U}^n)\mathrm{U}^n-\frac{1}{2}\mathrm{KU}^{n-1}\mathrm{U}^{n-1}\right]+\frac{\Delta t Gr}{Re^2}\mathrm{M}\cdot\Theta^n\delta_{\mathrm{i2}} \tag{8}$$

2.2. Viscosity phase

A first-order implicit Euler time integration scheme is applied here and a new intermediate velocity $\tilde{\mathrm{U}}^{n+1}$ is determined from $\hat{\mathrm{U}}^n$ by

$$\mathrm{M}\tilde{\mathrm{U}}^{n+1}=\mathrm{M}\hat{\mathrm{U}}^{n+1}-\Delta t\frac{1}{Re}\mathrm{S}(\tilde{\mathrm{U}}^{n+1}) \tag{9}$$

2.3. Pressure phase and incompressibility

In the phase, the final velocity field U^{n+1} is determined from the intermediate velocity $\tilde{\mathrm{U}}^{n+1}$ by adding the dynamic effect of the pressure P^{n+1}, which is determined so as to satisfy the incompressibility condition. This result is the following equation:

$$\mathrm{AP}^{n+1}=-\frac{1}{\Delta t}\mathrm{D}\tilde{\mathrm{U}}^{n+1} \tag{10}$$

The final velocity is consequently computed:

$$\mathrm{M}_D\mathrm{U}^{n+1}=\mathrm{M}_D\tilde{\mathrm{U}}^{n+1}-\Delta t\mathrm{HP}^{n+1} \tag{11}$$

where M_D is the diagonalized mass matrix obtained simply by summing across each row of the consistent mass matrix and placing the results in the diagonal.

2.4. Temperature phase

In the last phase, the temperature solutions can be obtained from the energy equation by applying the same procedure as the velocity phase.

$$\mathrm{M}\Theta^{n+1}=\mathrm{M}\Theta^n-\Delta t\left[\tfrac{3}{2}\mathrm{KU}^n\Theta^n-\tfrac{1}{2}\mathrm{KU}^{n-1}\Theta^{n-1}\right]-\frac{\Delta t}{RePr}\mathrm{A}\Theta^{n+1}+\frac{\Delta t}{RePr}\mathrm{Q}^n \tag{12}$$

We impose the 'traction free' condition instead of $\mathrm{P}=0$ at one point in the outflow plane. The equation of the outflow boundary condition for pressure can be adopted as used by Ramaswamy and Jue [16]. As usual, a physical quantity of great interest is the local Nusselt number Nu along the surfaces of the solid walls. The definition of Nu has been given as

$$Nu=-\frac{1}{\theta_{\mathrm{w}}}\frac{\partial\theta}{\partial n}$$

where n denotes normal to the solid surface.

The primary purpose of this development is to remove the direct treatment of a large scale matrix created by coupled nonlinear equations and to solve the coupled Navier–Stokes equations and energy equation in a

sequential procedure. The intention is to save the memory storage and make an efficient computation. Quadrilateral elements with four nodes are used here over triangular elements to obtain good accuracy with a limited number of nodes. The elemental matrices are computed only once and used again at each time step. The skyline method was adopted for the storage of global matrices to reduce storage requirements. A direct solver of LU factorization based on Gaussian elimination technique was developed to deal with a symmetric banded system.

3. Results and discussion

A detailed numerical study has been carried out on mixed convection heat transfer enhancement by placing an oblique plate in a horizontal block-heated channel. In the study, the Grashof number is taken as 0, 8000 and 3 200 000 and the Reynolds numbers as 260, 400 and 530 when Prandtl number is kept constant at 0.7. All the calculations have been performed by using a HP 90000/730 computer. After a series of test runs, a finite-element mesh (3490 nodes and 3232 elements) was chosen for all cases. Further refinement changed the time-mean Nusselt number less than 0.05% for the test runs. The other two meshes tested are 2914 nodes (2680 elements) and 4300 nodes (4010 elements). The thickness of the oblique plate is so small to be treated as the width of one element but without mesh in the plate, so we can directly substitute no-slip conditions and zero temperature gradient into the nodes on the edges of the plate. The time increment Δt was set at 0.0008 in the calculations of unsteady flow and heat transfer over heated blocks with and without an oblique plate. The calculation for the case without an oblique plate utilized 10 000 time steps to reach steady flow and the computation time was about 7 h 47 min 58 s of CPU time. The calculation for the case with an oblique plate required 20 000 time steps to obtain the periodic vortex shedding and the computation times were about 20 h 6 min 59 s to 20 h 38 min 6 s of CPU time.

To show that the program can handle boundary step changes and natural convection flows, we apply the present method to solve the steady flow of laminar mixed convection in a vertical channel containing a block on one channel wall. The wall containing the block is assumed to be hot (constant temperature) while the other wall is assumed to be adiabatic. The steady-state solution is obtained by the time integration procedure as mentioned in the preceding section. As a convergence criterion, we consider the difference in the calculated velocity fields. The calculations were terminated when the solution for nodal velocity components varied less than 0.01% in the Euclidean norm between two consecutive time steps. A comparison of the present predictions agreeing fairly closely with Habchi and Acharya's predictions [17] as shown in Fig. 2 gives one confidence in the use of the present program.

In this study, time-mean Nusselt number is thereafter used for comparing the heat transfer characteristics between the case with an oblique plate and the case without an oblique plate. Time-mean Nusselt number for heated blocks with an oblique plate is calculated in time interval containing several flow cycles of vortex shedding, while time-mean Nusselt number for the case without an oblique plate is calculated in time interval approaching a steady flow. The time-mean Nusselt number along the block is presented in Fig. 3 for Gr/Re^2 values at $Re = 400$ in the channel flow over heated blocks. The local Nusselt number shows the same characteristic behavior that it increases with an increase in the Gr/Re^2 value. The maximum local Nusselt number for a given block occurs at the front corner; the minimum value occurs at the groove between two blocks. The influence of mixed convection is prominent along the vertical surfaces of the blocks. Moreover, from $Gr = 0$ to 3 200 000, change in time-mean Nusselt number for all the blocks is about 11.8% which can be calculated by using the values listed in Table 1. Similar observations have been seen in an earlier study [6]. These results can be explained from Fig. 4. In Fig. 4 the curvature of the streamline becomes very large locally at the corner ($x = 2.5$, $y = 0.5$); this has a high flow velocity, so the convective heat transfer is large. Figure 4 also shows that the recirculating zone behind the last block is larger when the Gr/Re^2 value becomes large. This behavior is expected since, for $Gr/Re^2 = 20$, the strong buoyant upflow along the vertical surfaces of the blocks (in y-direction) facilitates the size of the separated eddy. This result can provide confirmation to the flow processes.

The heat transfer enhancement of an oblique plate installed above the first block is shown in Fig. 5 for three Gr/Re^2 values at $Re = 400$. The distribution of time-mean Nusselt number along the block increases in comparison to the case without oblique plate as shown in Fig. 3. The buoyancy effect still appears along the vertical surfaces of the blocks. Figure 6 exhibits the flow fields for the corresponding instantaneous stream patterns each time at the peak of one vortex-shedding cycle. When Gr/Re^2 is less than $O(1)$ (Fig. 6(a) (b)), wave flows induced by vortex shedding behind the oblique plate pass stronger and faster over the first to the third block, then weaker and slower over the subsequent two blocks. The wave flows change the recirculating zone behind the last block from one into two. At $Gr/Re^2 = 20$ (Fig. 6(c)), the strong buoyant upflow along the vertical surfaces of the blocks interacts with the wave flows and strengthens these flows across the blocks. On the other hand, the strong buoyant upflow enlarges the size of both recirculation zones. On the whole, the wave flows can improve heat transfer along the block. Figure 7 shows the time-mean Nusselt number along the block surface without and with a plate of

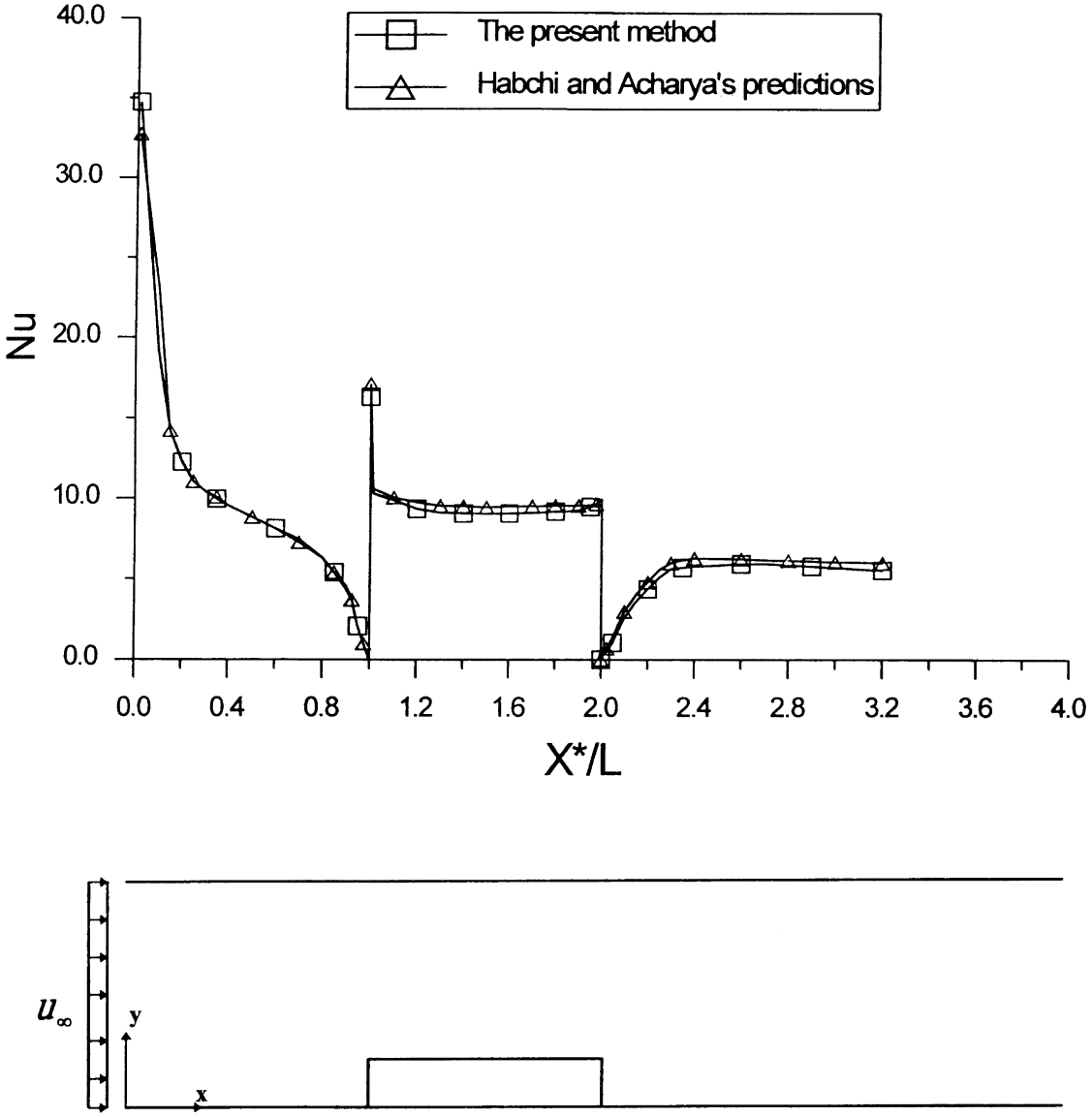

Fig. 2. Comparison between the present predictions and the Habchi and Acharya's predictions for $Re = 218$ and $Gr/Re^2 = 3$.

different oblique angles for $Gr = 3\,200\,000$, and $Re = 400$ ($Gr/Re^2 = 20$). The use of the oblique plate with various angles can increase the distribution of time-mean Nusselt number along the block surface. For various oblique angles, the instantaneous streamlines at the corresponding flow condition are shown in Fig. 8 each time at the peak point of one vortex-shedding cycle. Installing the oblique plate locally accelerates flow past the passageway between the plate and the first block but generates different patterns of wave motion induced by vortex shedding. The oscillations generated by the oblique plate can additionally assist heat transfer along the block surface. When Gr/Re^2 is larger than $O(1)$, the improvement in heat transfer is mainly as a result of the oscillations forcing the mainstream flow to mix with the buoyant upflow along the vertical surfaces of the blocks.

Vortex shedding generated by the oblique plate can additionally enhance heat transfer along the block surface. Coupled vortex shedding/mixed convection process is detailed and demonstrated in Figs 9 and 10, where we plot a sequence of instantaneous streamlines during the flow cycle for $Gr/Re^2 = 0.5$ and $Gr/Re^2 = 20$ at $Re = 400$. The flow in Fig. 9 is asymmetrically induced by placing the oblique plate between the upper channel-wall and the blocks. At $t = 12.984$, the upper vortex generates around the upper tip of the plate and the lower

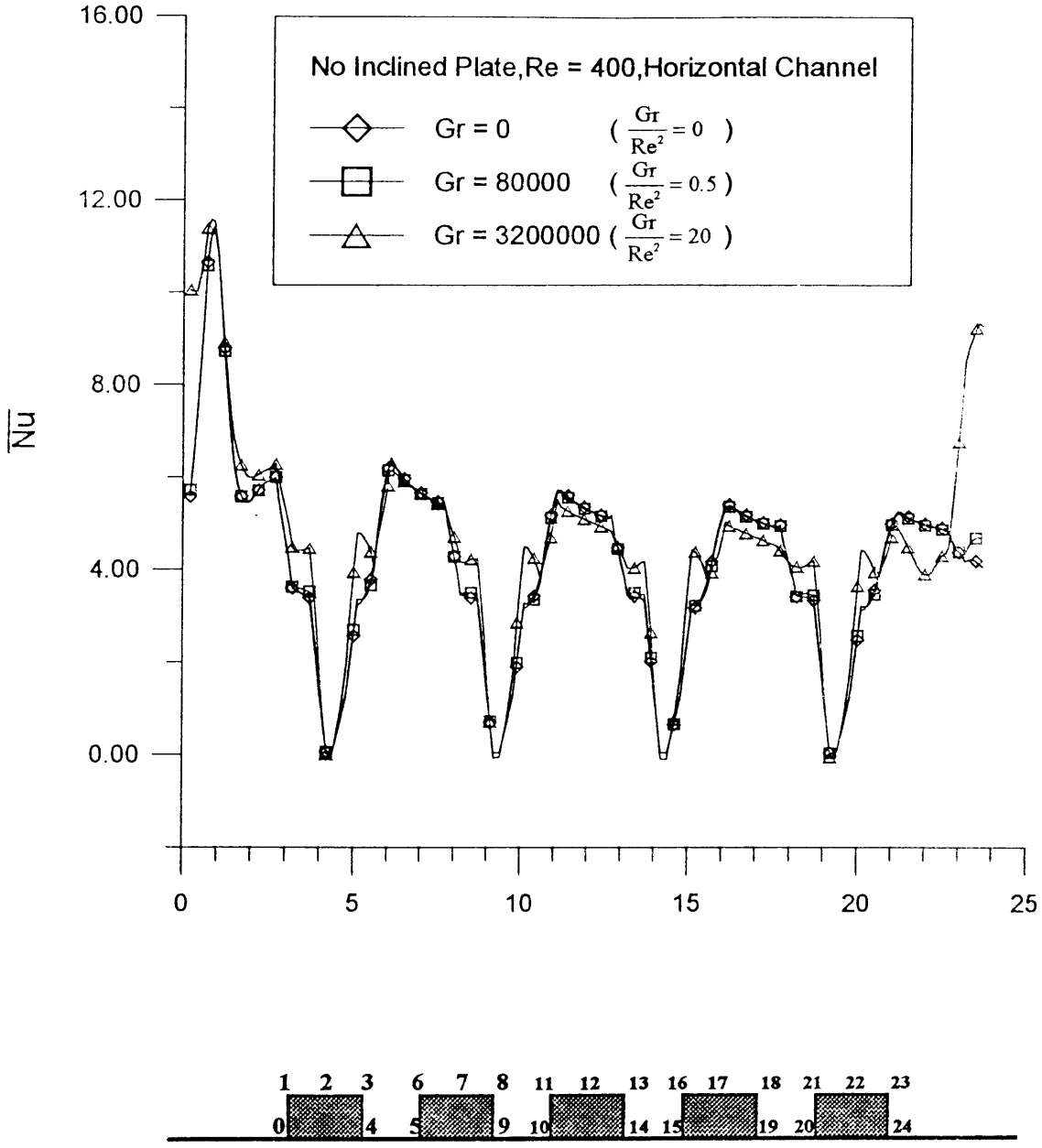

Fig. 3. Time-mean Nusselt number variation along the block surface for Gr/Re^2 values at $Re = 400$.

vortex leaves the trailing edge of the plate. The streamlines at $t = 14.384$ are similar to those at $t = 12.984$; this presents a cycle of the periodic vortex shedding. The oscillatory nature of the wake behind the oblique plate can be clearly seen in the streamlines. The same characteristics of the periodic vortex shedding are also shown in Fig. 10 for the case of $Gr/Re^2 = 20$ and $Re = 400$. Once the upward wave passes over the grooves between the blocks, the groove vortex is eject into the main flow stream as shown in Fig. 11(a) ($Gr/Re^2 = 0.5$). It is notable in Fig. 11(b) that, when the effects of natural convection are substantial, ($Gr/Re^2 = 20$) there appears a secondary vortex in the groove between the blocks. The secondary vortex rotates in the direction opposite to that of the original vortex between the blocks. The fluid rises upward in the vicinity of the vertical surface of the block under substantial buoyancy effects and its movement in addition to the upward wave passing over the groove as

Table 1
For three Gr/Re^2 values at $Re = 400$, values of average time-mean Nusselt number along the block without and with an oblique plate (note: values in parentheses designating the percentage change relative to no oblique plate)

	no oblique plate	ω		
		30°	60°	90°
for $Gr/Re^2 = 0$ at $Re = 400$				
first block	6.1242	7.6732 (25.3%)	8.1953 (33.8%)	8.2622 (34.9%)
second block	4.7170	6.1572 (30.5%)	6.9586 (47.5%)	5.8404 (23.8%)
third block	4.4516	4.8321 (8.5%)	5.3192 (19.5%)	4.2862 (−3.7%)
fourth block	4.3033	4.3832 (1.9%)	4.4966 (4.5%)	4.1333 (−4.0%)
fifth block	4.4224	4.4087 (−0.3%)	4.4046 (−0.4%)	4.2198 (−4.6%)
over all block	4.8037	5.4909 (13.2%)	5.8749 (21.0%)	5.3484 (9.3%)
for $Gr/Re^2 = 0.5$ at $Re = 400$				
first block	6.1467	8.1527 (32.6%)	8.5346 (38.8%)	8.3125 (35.3%)
second block	4.7173	6.5237 (38.3%)	7.1473 (51.5%)	6.3273 (34.1%)
third block	4.4522	5.4298 (22.0%)	5.6009 (25.8%)	4.4071 (−1.0%)
fourth block	4.3048	5.0445 (17.2%)	4.6970 (9.1%)	4.1922 (−2.6%)
fifth block	4.4953	5.2055 (15.8%)	4.3543 (−3.1%)	4.4629 (−0.7%)
over all block	4.8233	6.0712 (25.2%)	6.0668 (24.4%)	5.5404 (13.0%)
for $Gr/Re^2 = 20$ at $Re = 400$				
first block	7.2900	8.9419 (22.7%)	9.5621 (31.2%)	9.4246 (29.3%)
second block	5.0754	7.1838 (41.5%)	7.9802 (57.2%)	6.7640 (33.3%)
third block	4.6439	5.8602 (26.2%)	6.2397 (34.4%)	5.8353 (25.7%)
fourth block	4.4166	5.2305 (18.4%)	6.4157 (45.3%)	5.6172 (27.2%)
fifth block	5.4249	6.4831 (19.5%)	7.0317 (29.6%)	6.4467 (18.8%)
over all block	5.3701	6.7399 (25.7%)	7.4459 (39.5%)	6.8176 (26.9%)

mentioned above may make the groove vortex ejected more into the main stream. This generates a counter-rotating vortex near the forward face of the rearward-located block to change the shape of the original groove vortex and shift the location to the forward-located block. Figure 12 shows the variation of the pressure coefficient for the oblique plate. The Strouhal number is defined by

$$St = \frac{\mathrm{d}(\sin\omega) f_s}{u_\infty}$$

$St = 0.2760$ is for $Re = 400$ and $Gr = 80\,000$, and $St = 0.2798$ is for $Re = 400$ and $Gr = 3\,200\,000$. Other numerical and experimental studies have been not been found to compare with the numerical work presented here. However, Lugt and Haussling [18] obtained $St = 0.1770$ for a uniformly incoming flow past an oblique plate of angle 45° for $Re = 200$.

We may investigate the influence of oblique angle of the plate on heat transfer enhancement by means of the values of average time-mean Nusselt number for the blocks as follows. The average time-mean Nusselt number is calculated by the values of time-mean Nusselt number on all nodes of the block boundary. The value of average time-mean Nusselt number for the blocks are listed in Table 1 for various oblique angles of the plate as well as for no oblique plate when Gr/Re^2 value changes at $Re = 400$. The value of average time-mean Nusselt number for all the blocks increases with increasing Grashof number for the oblique plate as well as for no oblique plate. The maximum value of average time-mean Nusselt number appears at the first block, and the value decreases progressively for the subsequent three blocks. The value of average time-mean Nusselt number for all the blocks increases with installing the oblique plate in comparison to no oblique plate. The maximum value of average time-mean Nusselt number for the whole block occurs at $\omega = 60°$ with $Gr/Re^2 = 20$. As also shown in parentheses in Table 1, the maximum increase in time-mean overall average Nusselt number is 39.5% when the oblique angle is 60° with $Gr/Re^2 = 20$. For Gr/Re^2 less than $O(1)$, the increase in the overall average Nusselt number at $\omega = 30°$ is larger than the increase at $\omega = 90°$; this result is primarily contributed by an increase in the

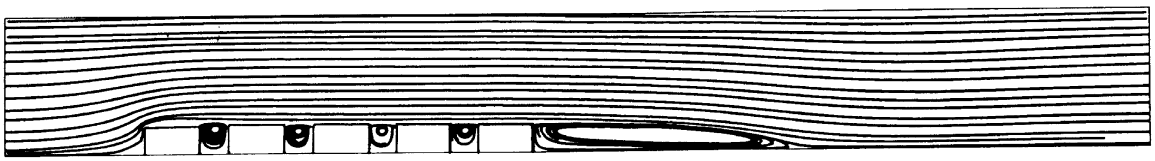

(a)

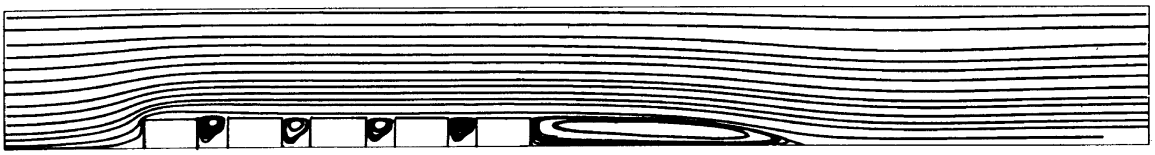

(b)

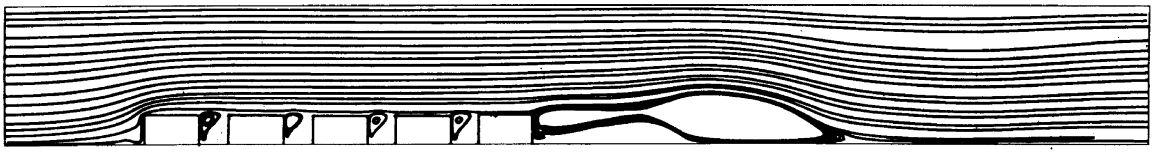

(c)

Fig. 4. Stream patterns for $Re = 400$: (a) $Gr/Re^2 = 0$, (b) $Gr/Re^2 = 0.5$, (c) $Gr/Re^2 = 20$.

average time-mean Nusselt number along the second to the fourth block (Table 1), because the oscillations effectively improve the heat transfer. In the contrast, for $Gr/Re^2 = 20$, the increase at $\omega = 90^\circ$ is slightly larger than the increase at $\omega = 30^\circ$. This result is primarily contributed by an increase in the average time-mean Nusselt number, only along the first and the fourth block (Table 1), because the buoyant upflow along the vertical surfaces of the block effectively strengthens the oscillations (Fig. 8(c)). The value of average time-mean Nusselt number for the block are summarized in Table 2 for various oblique angles of the plate and no oblique plate as Reynolds number changes at $Gr = 3\,200\,000$. The value of average time-mean Nusselt number for the block

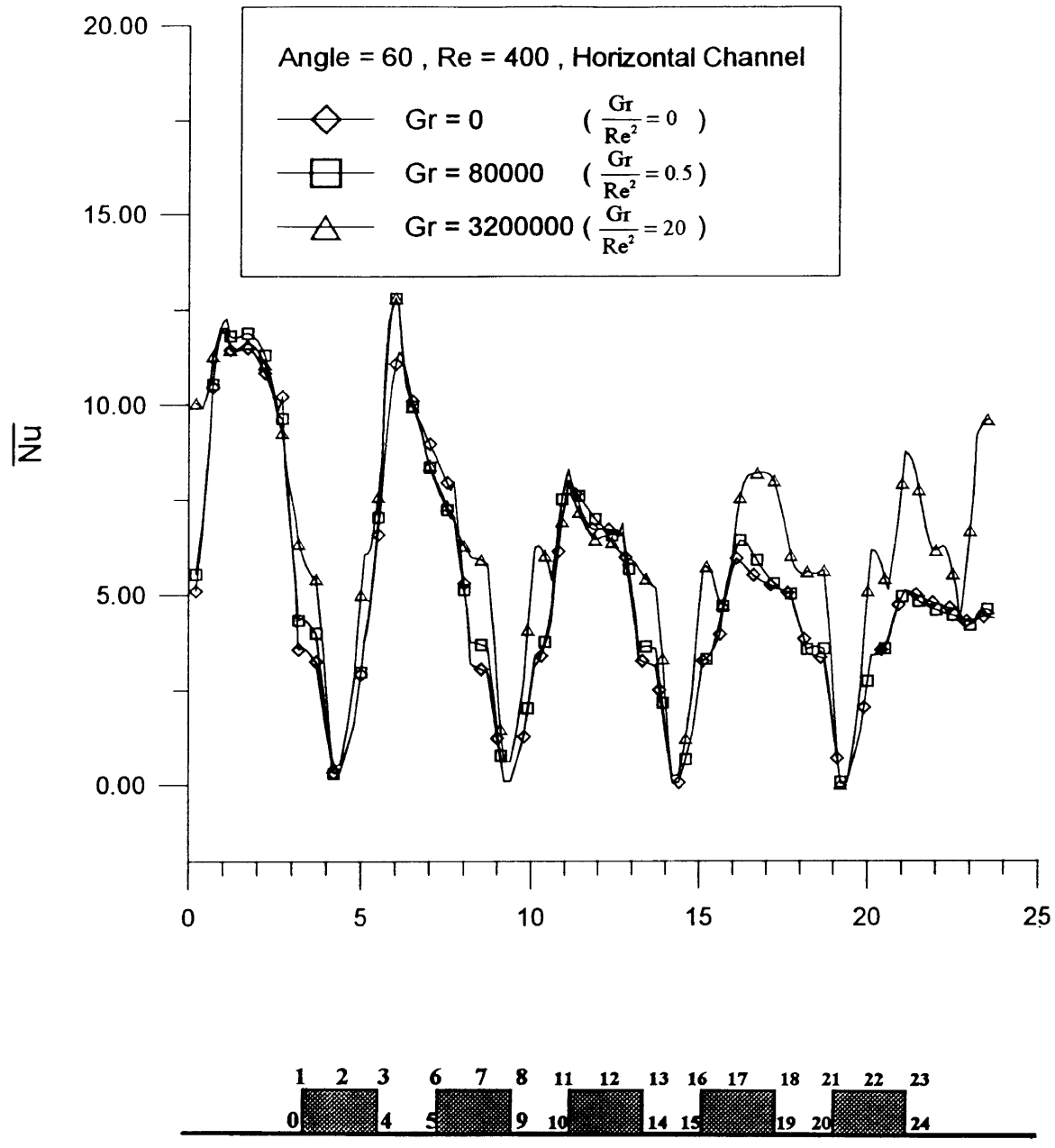

Fig. 5. Effect of Gr/Re^2 values on time-mean Nusselt profiles installing an oblique plate ($\omega = 60^\circ$) at $Re = 400$.

increases with increasing Reynolds number for the oblique plate as well as for no oblique plate. The value of average time-mean Nusselt number for the whole block increases with installing the oblique plate in comparison to no oblique plate. The maximum value of average time-mean Nusselt number for the whole block appears at $\omega = 60^\circ$ for $Re = 530$. On the contrary, as shown in parentheses in Table 2, the maximum increase in time-mean overall average Nusselt number is 57.1% at $\omega = 90^\circ$ with $Re = 260$ ($Gr/Re^2 = 47$) because of the small time-mean overall average value for no oblique plate.

4. Conclusion

Numerical investigation has been systematically performed on the unsteady flow and mixed convective heat

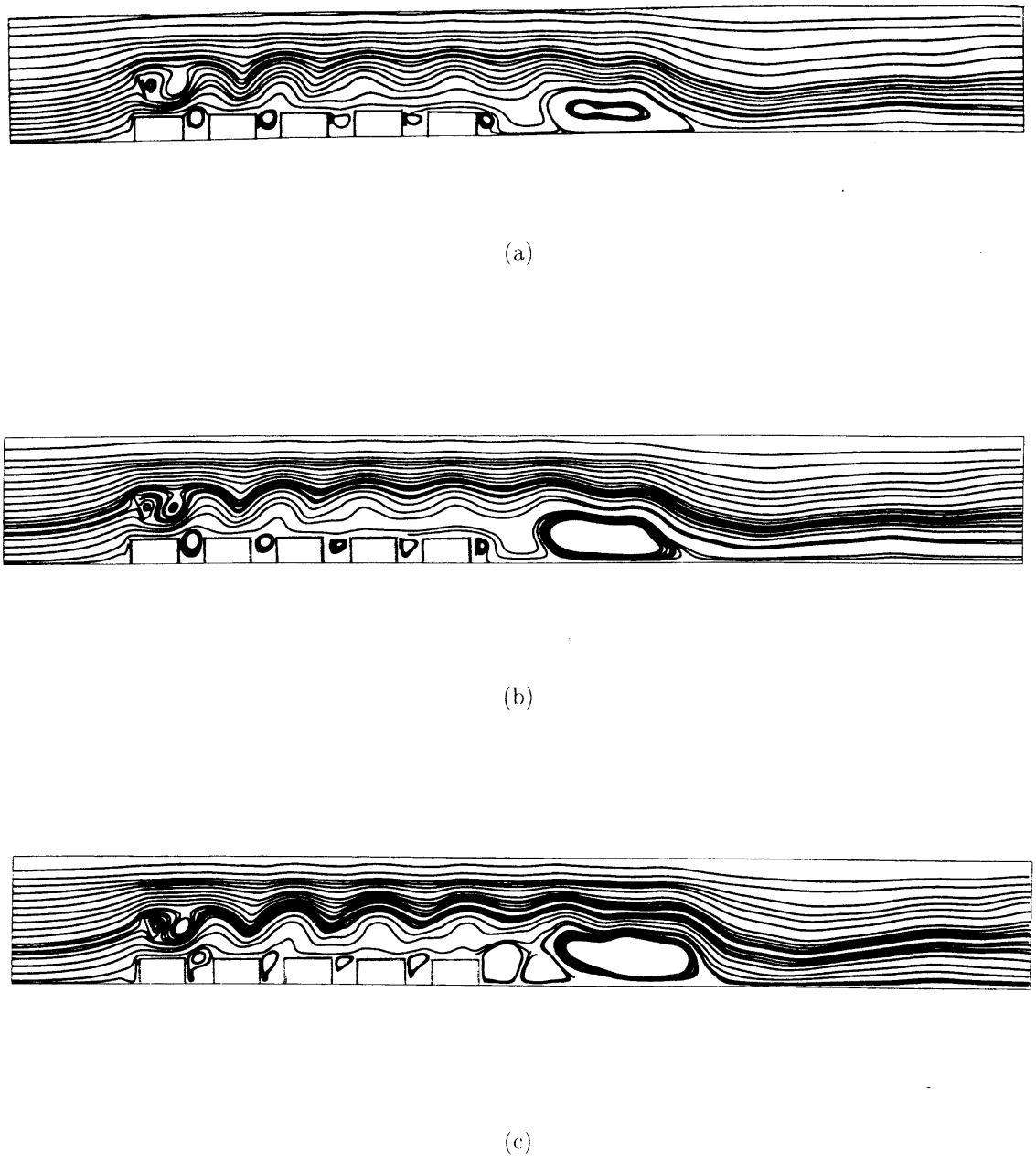

Fig. 6. Stream patterns installing an oblique plate ($\omega = 60^\circ$) for $Re = 400$: (a) $Gr/Re^2 = 0$, (b) $Gr/Re^2 = 0.5$, (c) $Gr/Re^2 = 20$.

transfer in a horizontal block-heated channel with and without installing an oblique plate above an upstream block. On the basis of these results presented and discussed in the discussion section, we draw the main conclusions below.

(1) Installing an oblique plate can effectively improve the heat transfer characteristics through the modification of the flow pattern.
(2) Coupling the buoyancy effects and vortex shedding has profound influences in determining the unsteady fields and heat transfer characteristics.
(3) The buoyancy effects still exists along the vertical surfaces of the blocks with an oblique plate ($\omega = 60^\circ$) for three Gr/Re^2 values.
(4) When Gr/Re^2 is less than $O(1)$, wave flows induced by vortex shedding behind the oblique plate pass stronger and faster across the first to the third block,

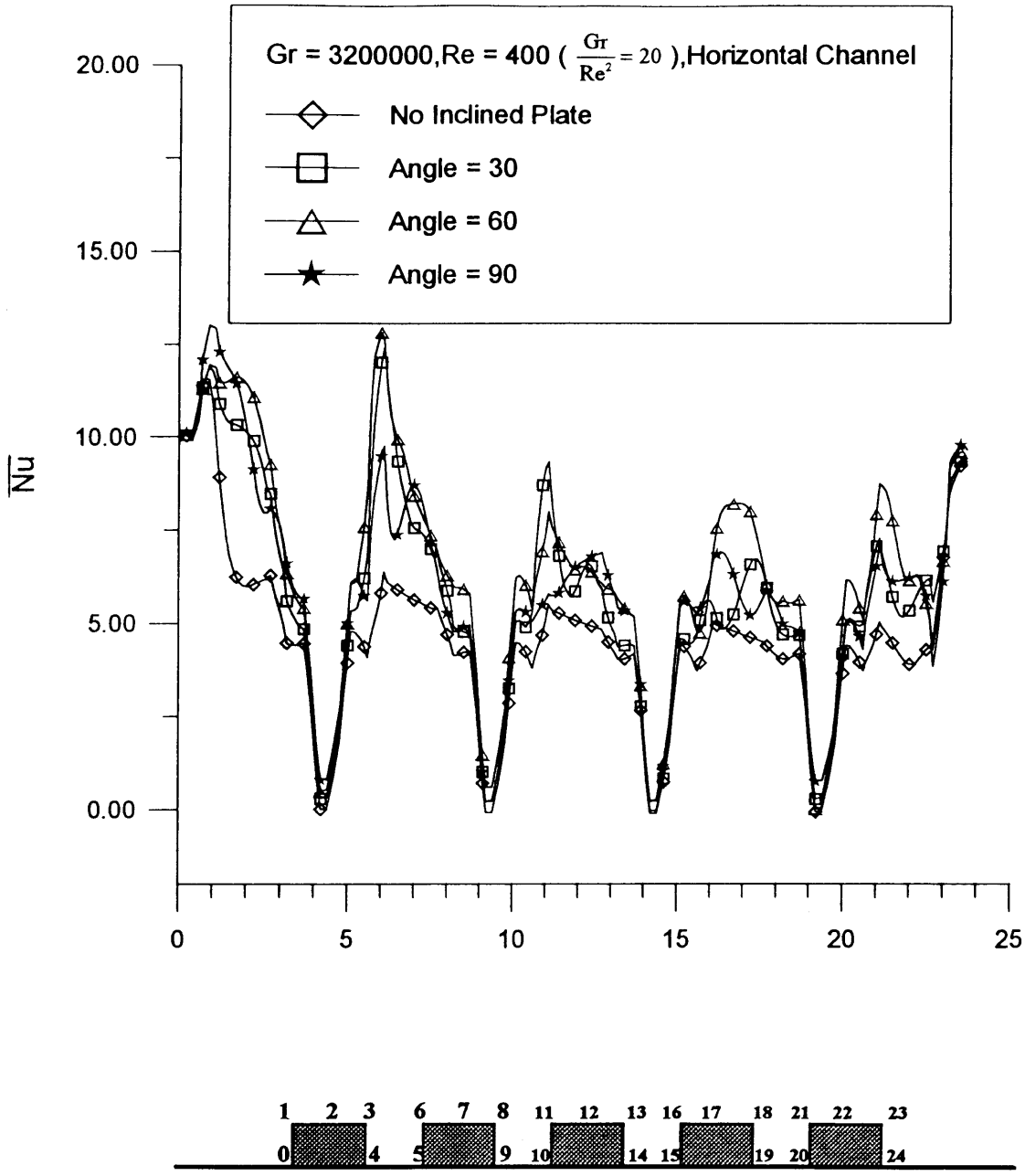

Fig. 7. Influence of oblique angles on time-mean Nusselt number profiles compared to no plate at $Gr = 3\,200\,000$ and $Re = 400$.

then weaker and slower over the subsequent two blocks. The wave flows change the recirculating zone behind the last block from one into two.

(5) At $Gr/Re^2 = 20$, the strong buoyant upflow along the vertical surfaces of the blocks interacts with the wave flows and strengthens these flows across the blocks.

(6) For three Gr/Re^2 values at a fixed value of Reynolds number, the maximum increase in time-mean overall average Nusselt number is 39.5% when the oblique angle is 60° with $Gr/Re^2 = 20$.

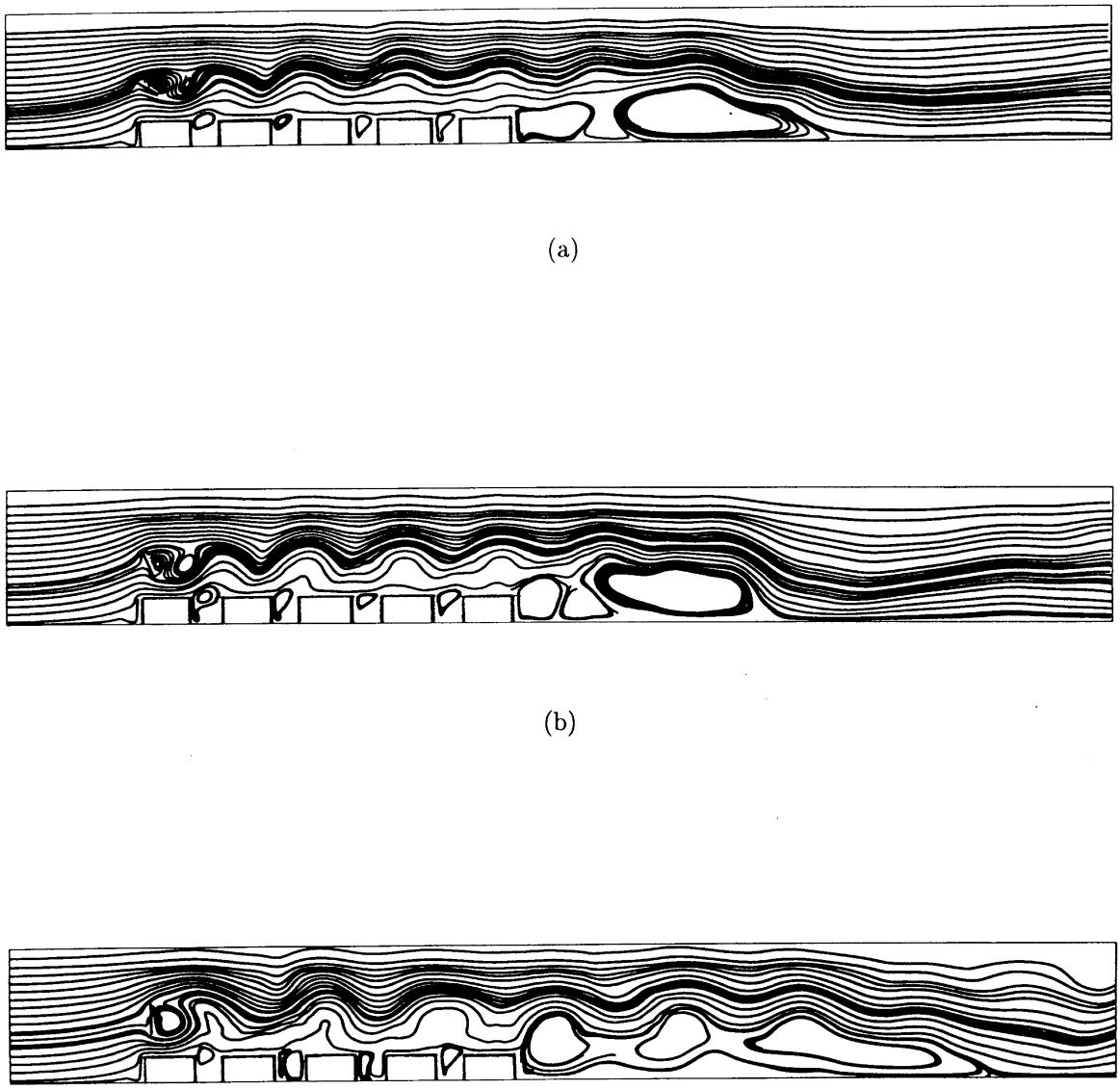

Fig. 8. Stream patterns for various oblique angles at $Gr = 3\,200\,000$ and $Re = 400$: (a) $\omega = 30^\circ$, (b) $\omega = 60^\circ$, (c) $\omega = 90^\circ$.

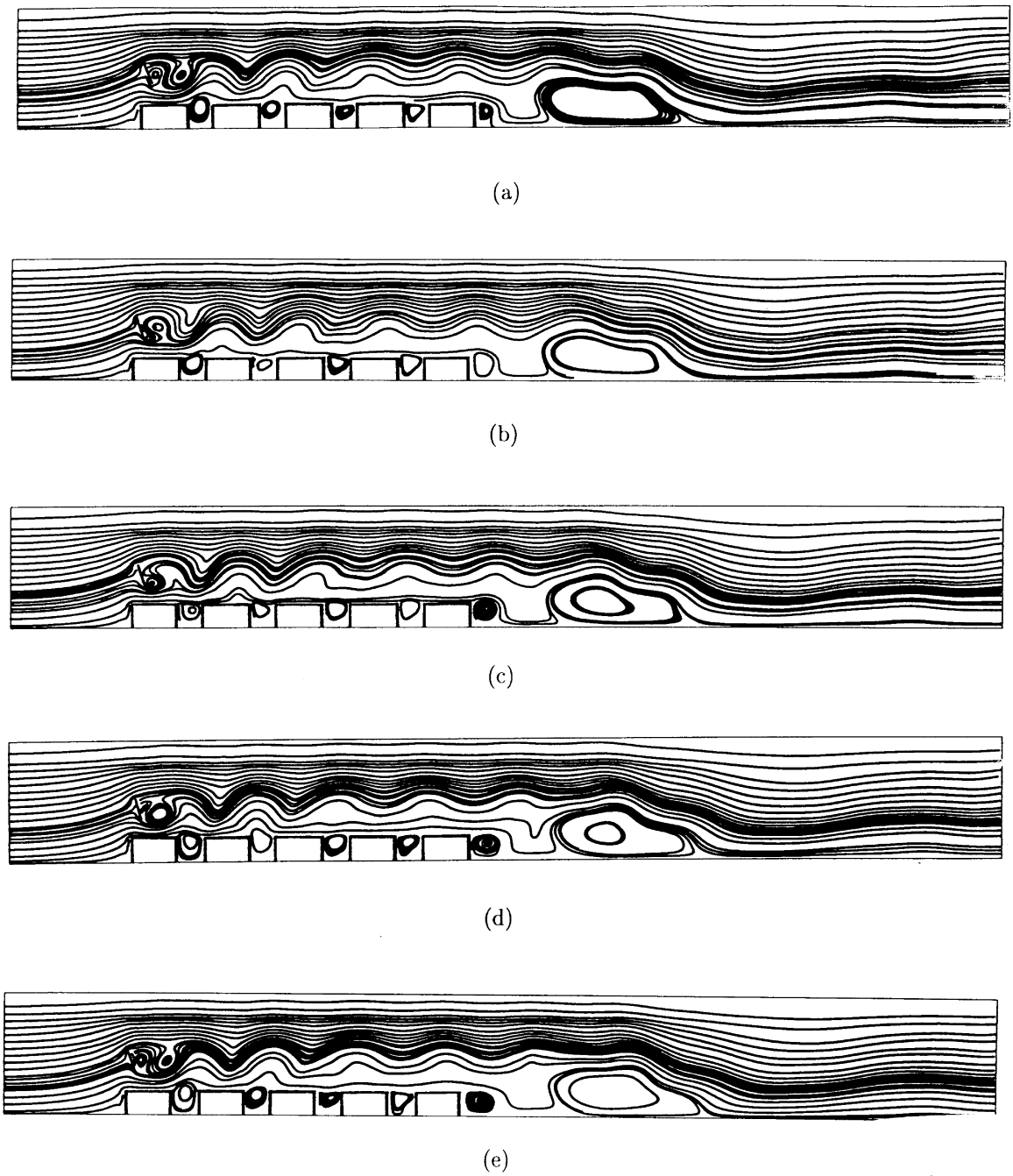

Fig. 9. Sequence of streamlines with an oblique plate ($\omega = 60^\circ$) during one cycle at (a) $t = 12.984$, (b) $t = 13.332$, (c) $t = 13.68$, (d) $t = 14.032$, (e) $t = 14.384$ for $Gr/Re^2 = 0.5$ and $Re = 400$.

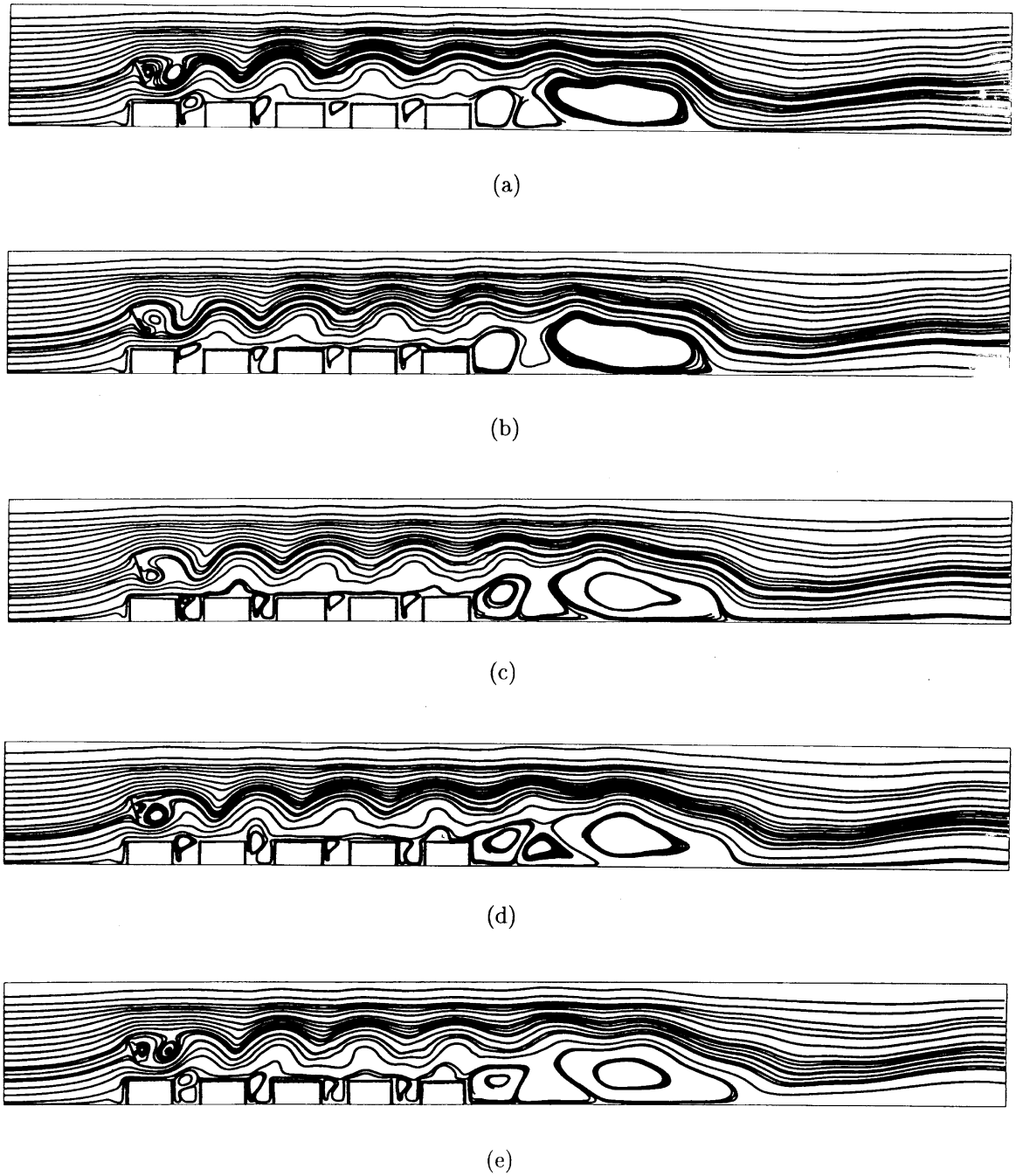

Fig. 10. Sequence of streamlines with an oblique plate ($\omega = 60^{\circ}$) during one cycle at (a) $t = 12.928$, (b) $t = 13.272$, (c) $t = 13.616$, (d) $t = 13.964$, (e) $t = 14.312$ for $Gr/Re^2 = 20$ and $Re = 400$.

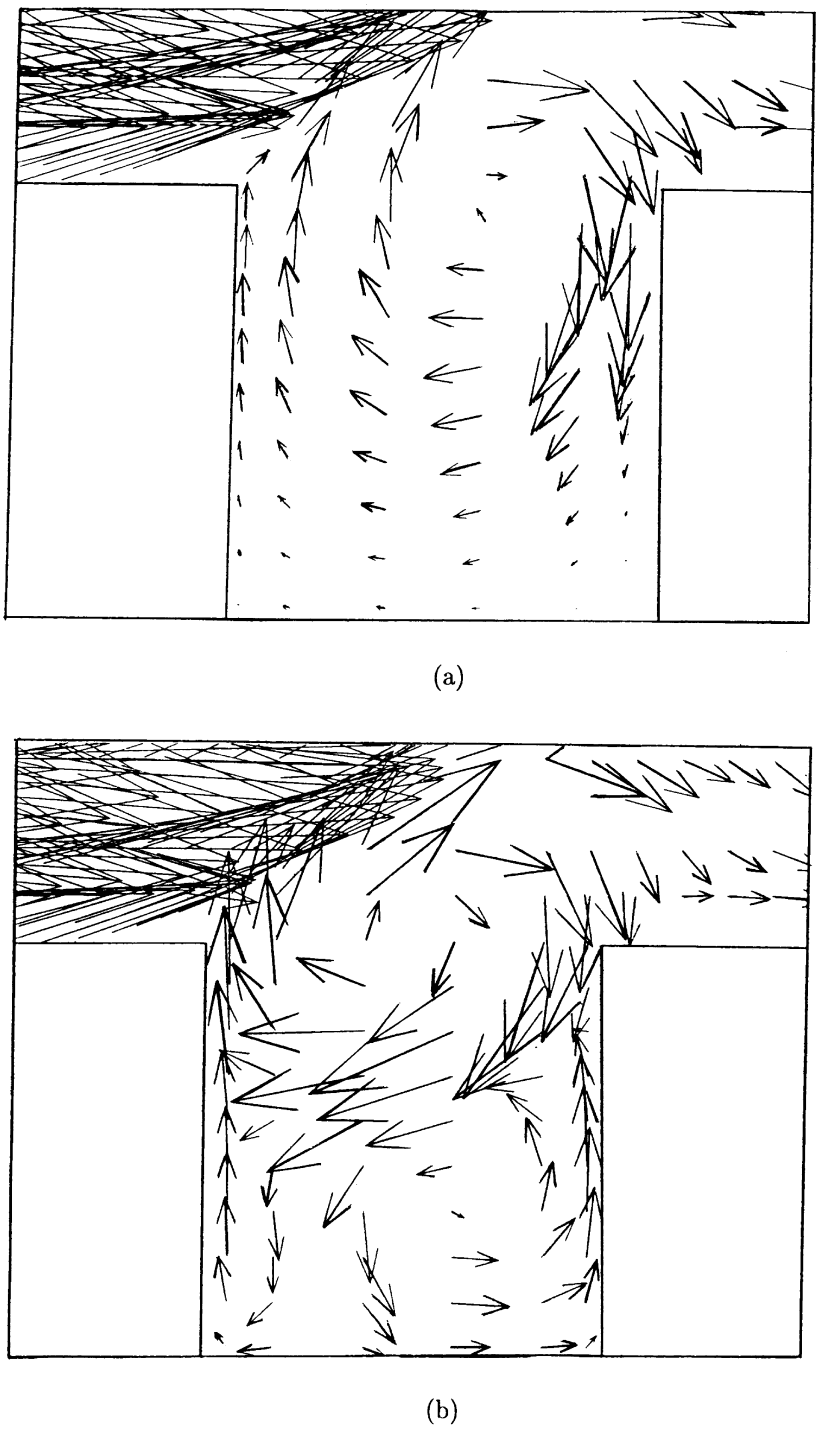

Fig. 11. Velocity vector enlarged in the first groove and its vicinity for $Re = 400$: (a) at $t = 12.984$ for $Gr/Re^2 = 0.5$ and $Re = 400$, (b) at $t = 12.928$ for $Gr/Re^2 = 20$ and $Re = 400$.

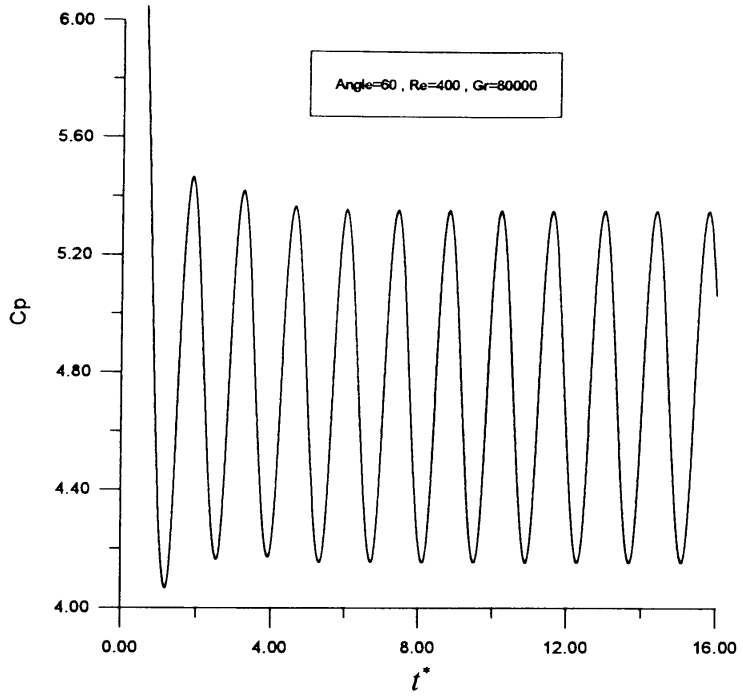

(a)

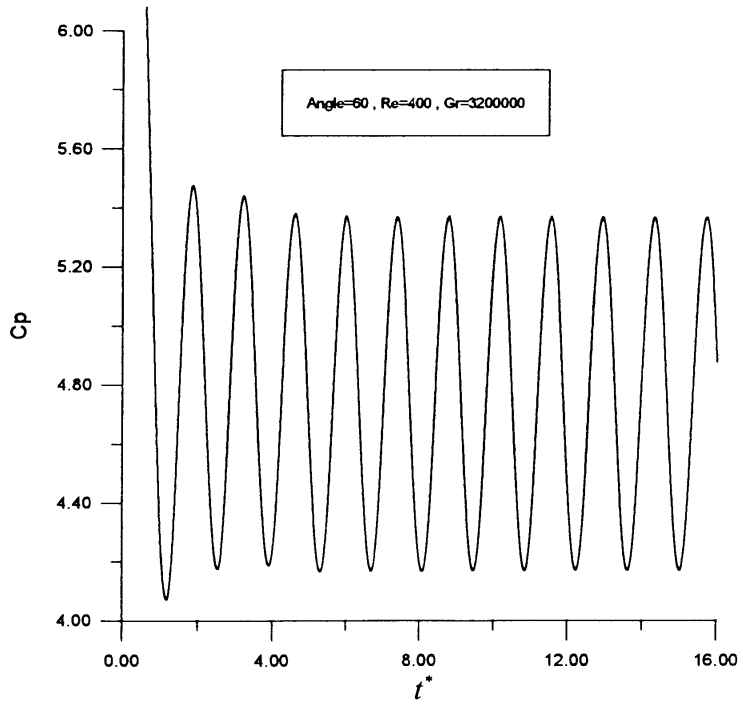

(b)

Fig. 12. Pressure coefficient C_p vs time for (a) $Gr/Re^2 = 0.5$ and (b) $Gr/Re^2 = 20$ at $Re = 400$.

Table 2
For three Reynolds number at $Gr = 3\,200\,000$ values of average time-mean Nusselt number along the block without and with an oblique plate (note: values in parentheses designating the percentage change relative to no oblique plate)

	no oblique plate	ω		
		30°	60°	90°
For $Re = 260$				
at $Gr = 3\,200\,000$				
first block	7.1899	8.2472 (14.7%)	8.8160 (22.6%)	8.7441 (21.6%)
second block	4.3645	6.4077 (46.8%)	6.9027 (58.2%)	7.0948 (62.6%)
third block	3.8997	6.1421 (57.5%)	6.5131 (67.0%)	6.8750 (76.3%)
fourth block	3.7691	6.3409 (68.2%)	6.3888 (69.5%)	7.0875 (88.0%)
fifth block	5.2966	7.7310 (46.0%)	7.4966 (41.5%)	7.2515 (36.9%)
over all block	4.9039	6.9738 (46.6%)	7.2234 (51.8%)	7.4106 (57.1%)
for $Re = 400$				
at $Gr = 3\,200\,000$				
first block	7.2900	8.4419 (22.7%)	5.9620 (31.2%)	9.4246 (29.3%)
second block	5.0754	7.1838 (41.5%)	7.9802 (57.2%)	6.7640 (33.3%)
third block	4.6439	5.8602 (26.2%)	6.2397 (34.4%)	5.8353 (25.7%)
fourth block	4.4166	5.2305 (18.4%)	6.4157 (45.3%)	5.6172 (27.2%)
fifth block	5.4249	6.4831 (19.5%)	7.0317 (29.6%)	6.4467 (18.8%)
over all block	5.3701	6.7399 (25.7%)	7.4459 (39.5%)	6.8176 (26.9%)
for $Re = 530$				
at $Gr = 3\,200\,000$				
first block	7.5128	9.6344 (28.2%)	10.2179 (36.0%)	9.9835 (32.9%)
second block	6.1126	8.1961 (34.1%)	8.8725 (45.1%)	7.8743 (28.8%)
third block	6.0213	7.1982 (19.5%)	7.2440 (20.3%)	7.3507 (22.1%)
fourth block	5.8941	6.5508 (9.4%)	8.1626 (36.3%)	6.7675 (13.0%)
fifth block	6.8941	7.1541 (3.8%)	8.1264 (17.9%)	7.1400 (3.6%)
over all block	6.5057	7.9467 (19.0%)	8.5247 (31.1%)	7.8232 (20.1%)

Acknowledgement

The authors gratefully acknowledge the partially financial support of this project by the National Council of the Republic of China.

References

[1] S. Oktay, H.C. Kamerer, A conduction-cooled module for high-performance LSI devices, IBM J. Res. Develop. 26 (1982) 55–66.
[2] R.C. Chu, U.P. Hwang, R.E. Simons, Conduction cooling for an LSI package: a one-dimensional approach, IBM J. Res. Develop. 26 (1982) 45–54.
[3] K.J. Kennedy, A. Zebib, Combined free and forced convection between horizontal parallel plates: some case studies, Int. J. Heat Mass Transfer 26 (1983) 471–474.
[4] B.H. Kang, Y. Jaluria, S.S. Tewari, Mixed convection air cooling of an isolated rectangular heat source module on a horizontal plate, ASME Proc., National Heat Transfer Conf. (1988) 59–66.
[5] M.E. Bratten, S.V. Patankar, Analysis of laminar mixed convection in shrouded arrays of heated rectangular blocks, Int. J. Heat Mass Transfer 28 (1980) 1699–170.
[6] S.Y. Kim, H.J. Sung, J.M. Hyun, Mixed convection from multiple-layered boards with cross-streamwise periodic boundary conditions, Int. J. Heat Mass Transfer 35 (1992) 2941–2952.
[7] E.M. Sparrow, S.B. Vemuri, D.S. Kadle, Enhanced and local heat transfer, pressure drop, and flow visualization, Int. J. Heat Mass Transfer 26 (1983) 689–699.
[8] T. Myrum, S. Acharya, S. Sinha, X. Qiu, Flow and heat transfer in a ribbed duct with vortex generators, ASME Journal of Heat Transfer 118 (1996) 294–300.
[9] T. Myrum, S. Acharya, A. Mehrotra, S. Inamdar, Vortex-generator induced heat transfer augmentation past a rib, ASME Journal of Heat Transfer 114 (1992) 280–284.
[10] T.A. Myrum, X. Qiu, S. Acharya, Heat transfer enhancement in a ribbed duct using vortex generators, International Journal of Heat Mass Transfer 36 (1993) 3497–3508.
[11] E. Ratts, C.H. Amon, B.B. Mikic, A.T. Patera, Cooling enhancement of forced convection air cooled chip array through flow modulation induced by vortex-shedding cylinders in cross-flow, In Win Aung (Ed.), Cooling Technology for Electronic Equipment, Hemisphere Publishing Corporation, New York, 1988, pp. 183–194.

[12] J.H. Chou, J. Lee, Reducing flow non-uniformities in LSI packages by vortex generator, In Win Aung (Ed.), Cooling Technology for Electronic Equipment, Hemisphere Publishing Corporation, New York, 1988, pp. 113–124.
[13] G.E. Karniadakis, B.B. Mikic, A.T. Patera, Heat transfer enhancement by flow destablization: application to the cooling of chips, In Win Aung (Ed.), Cooling Technology for Electronic Equipment, Hemisphere Publishing Corporation, New York, 1988, pp. 587–610.
[14] J.S. Nigen, C.H. Amon, Forced convective cooling enhancement of electronic package configurations through self-sustained oscillatory flows, Transactions of the ASME, Journal of Electronic Packaging 115 (1993) 356–365.
[15] B. Ramaswamy, T.C. Jue, J.E. Akin, Semi-implicit and explicit finite element schemes for coupled fluid/thermal problems, Int. J. Numer. Methods Eng. 34 (1992) 675–696.
[16] B. Ramaswamy, T.C. Jue, Some recent trends and developments in finite element analysis for incompressible thermal flows, Int. J. Numer. Methods Eng. 35 (1992) 671–707.
[17] S. Habchi, S. Acharya, Laminar mixed convection in a partially blocked vertical channel, Int. J. Heat Mass Transfer 29 (1986) 1711–1722.
[18] H.T. Lugt, H.J. Haussling, Laminar flow past an abruptly accelerated elliptic cylinder at 45° incidence, J. Fluid Mech. 65 (1974) Part 4 711–734.